Front. Energy 2020, 14(4): 836–849
https://doi.org/10.1007/s11708-017-0444-z

RESEARCH ARTICLE

Abdelkarim AMMAR, Amor BOUREK, Abdelhamid BENAKCHA

Robust SVM-direct torque control of induction motor based on sliding mode controller and sliding mode observer

Abstract This paper proposes a design of control and estimation strategy for induction motor based on the variable structure approach. It describes a coupling of sliding mode direct torque control (DTC) with sliding mode flux and speed observer. This algorithm uses direct torque control basics and the sliding mode approach. A robust electromagnetic torque and flux controllers are designed to overcome the conventional SVM-DTC drawbacks and to ensure fast response and full reference tracking with desired dynamic behavior and low ripple level. The sliding mode controller is used to generate reference voltages in stationary frame and give them to the controlled motor after modulation by a space vector modulation (SVM) inverter. The second aim of this paper is to design a sliding mode speed/flux observer which can improve the control performances by using a sensorless algorithm to get an accurate estimation, and consequently, increase the reliability of the system and decrease the cost of using sensors. The effectiveness of the whole composed control algorithm is investigated in different robustness tests with simulation using Matlab/Simulink and verified by real time experimental implementation based on dS pace 1104 board.

Keywords induction motor, direct torque control (DTC), space vector modulation (SVM), sliding mode control (SMC), sliding mode observer (SMO), dS1104

1 Introduction

Direct torque control (DTC) was presented is 80 s and it attracted the attention of researchers due to its many advantages, especially the simple structure and fast dynamic response [1–3]. The DTC scheme achieves decoupled control of the stator flux and the electromagnetic torque in stator reference frame by using a switching look-up table. DTC does not need axes transformation or current regulators contrary to field oriented control and it is less dependent on the machine parameters [4]. However, the basic DTC strategy uses hysteresis controllers for torque and flux error to select the appropriate switching vectors by using a switching look-up table. This presents an observed flux and torque ripples which produce acoustical noises and make control difficult at very low speed, in addition to variable switching frequency and high total harmonic distortion (THD) phase current [3–5].

Recently, several methods have been proposed to minimize these drawbacks. The well-used solution for ripples reduction is the use of space vector modulation. It can provide a constant switching frequency. The DTC method based on SVM, called SVM-DTC, can take various structures such as stator flux oriented control (SFOC) with SVM. This technique replaces hysteresis controllers by two (PI) controllers to generate the direct and the quadrature voltage components in *d-q* frame [6,7]. Another method, known as the closed loop torque control, is based on the changes of the torque of the motor. It achieves an appropriate voltage vector by use of a PI controller and a flux calculator [8].

It seems that all the aforementioned modified methods move a bit away from the principles of DTC. For example, they are based on PI controllers and non-stationary frame with coordination transformation in the SFOC method. In this case, the model of the system must be known. Besides, due to the using of PI controllers, the dynamic performance and stability of the system will be influenced by parameter variations, and therefore, the robustness will be wasted. Moreover, since the machine parameters are obtained by classical identification experiments, the measurement errors cannot be avoided. Furthermore, the value of

Received May 6, 2016; accepted July 4, 2016

Abdelkarim AMMAR (✉), Amor BOUREK, Abdelhamid BENAKCHA
LGEB Laboratory, Department of Electrical Engineering, University of Biskra, Biskra, BP 145, Algeria
E-mail: ammar.abdelkarim@yahoo.fr

parameters cannot be fixed because the physical properties are influenced by the environment condition. For example, the resistance varies with temperature or the inductance with saturation.

To overcome this problem, especially to enhance stability and robustness, different nonlinear and intelligent control methods such as fuzzy logic and neural networks [3], backstepping, feedback linearization and sliding mode control (SMC) [9–11] have been presented and applied to induction motor drives.

The SMC is a robust control method widely known in the automatic and control field. It forces the system trajectory to slide along the switching surface by determined control law [11–15]. The most powerful advantages of the SMC are robustness to parameter variations, rapid dynamic response, and simple software and hardware implementation [13,16]. Several works integrate SMC with DTC principles to achieve high performance control of induction motor [11,17].

In this paper, a sliding mode DTC SM-DTC with space vector modulation for IM drive is proposed to overcome most of the disadvantages of the conventional and SVM-DTC and obtain high control performance from both approaches, like low ripple level and fast dynamic with simplicity and robustness. Moreover, the previously mentioned control algorithm is developed in stationary frame.

Another aim of this paper is to apply sensorless application to disuse the mechanical sensors and reduce the cost of realization and installation of the system [18–20]. In this context, the observers remain an important area of research in this field. Many considerable researches have been suggested for electrical drives to estimate flux and rotor speed, such as model reference adaptive system, Kalman filtering or intelligence algorithms [4].

The SMC also proves its worth in this filed, and proves that it is applicable for both algorithm design, observers and controllers. The sliding mode observers (SMOs) are acknowledged by their robustness versus parameter variations. All these have been widely discussed [12,19,20]. In Section 6 in this paper, an inherently SMO is used to estimate flux and rotor speed. It is not a speed adaptive observer, therefore, it does not take the rotor speed as adaptive quantity contrary to known speed adaptive observers. This increases the accuracy and avoids the noise which affects the speed in estimation [14].

In this paper, an improved sliding mode DTC with SVM is presented. This control algorithm is accompanied with SMO for flux, speed and torque reconstruction. The results is examined and verified by simulation and real time experimentation based on dSpace 1104. The sampling frequency of the used dSpace 1104 can reach up to 20 kHz. As much as it minimizes, it reduces the output signals harmonics.

2 Induction motor model

The dynamic model equations of the induction motor will be defined in the stationary frame reference above. The state variables are represented by stator currents and flux as

$$\begin{cases} \dfrac{\mathrm{d}i_{s\alpha}}{\mathrm{d}t} = -\left(\dfrac{R_s}{\sigma L_s}+\dfrac{R_r}{\sigma L_r}\right)i_{s\alpha}-\omega_r i_{s\beta}+\dfrac{R_s}{\sigma L_s L_r}\psi_{s\alpha} \\ \qquad\qquad +\dfrac{\omega_r}{\sigma L_r}\psi_{s\beta}+\dfrac{1}{\sigma L_s}u_{s\alpha}, \\ \dfrac{\mathrm{d}i_{s\beta}}{\mathrm{d}t} = -\left(\dfrac{R_s}{\sigma L_s}+\dfrac{R_r}{\sigma L_r}\right)i_{s\beta}+\omega_r i_{s\alpha}+\dfrac{R_s}{\sigma L_s L_r}\psi_{s\beta} \\ \qquad\qquad -\dfrac{\omega_r}{\sigma L_r}\psi_{s\alpha}+\dfrac{1}{\sigma L_s}u_{s\beta}, \\ \dfrac{\mathrm{d}\psi_{s\alpha}}{\mathrm{d}t} = u_{s\alpha}-R_s i_{s\alpha}, \\ \dfrac{\mathrm{d}\psi_{s\beta}}{\mathrm{d}t} = u_{s\beta}-R_s i_{s\beta}, \end{cases} \tag{1}$$

where $i_{s\alpha}$ and $i_{s\beta}$ are stator current components, $\psi_{s\alpha}$ and $\psi_{s\beta}$ are stator flux components, R_s and R_r are stator and rotor resistances, and L_s and L_r are stator and rotor inductances.

$\sigma = 1-\dfrac{M_{sr}}{L_s L_r}$ is Blondel's coefficient and M_{sr} is the mutual stator-rotor inductance.

The electromagnetic torque is expressed by

$$T_e = p(\psi_{s\alpha} i_{s\beta}-\psi_{s\beta} i_{s\alpha}), \tag{2}$$

where p is the number of poles pairs.

3 Sliding mode direct torque control design

To select voltage vectors, the classical DTC control scheme uses the hysteresis controllers which raise the torque and flux ripples level. Furthermore, the modified SVM-DTC is based on PI controllers to generate voltage reference in (d-q) frame. Consequently, it needs reference transformation which increases control scheme complexity. In addition, it may be sensitive to parameter variation.

In order to overcome the drawbacks of both aforementioned algorithms, the SMC is used with the same variables used in DTC (SM-DTC). This method ensures a decoupled stator flux and torque control without any coordinate transformation or oriented axis, unlike the stator flux oriented (SFOC) DTC-SVM. SM-DTC is based on tracking errors of the torque and flux to generate the stator voltage command [21]. It can considerably reduce the complexity of SVM-DTC by using the stationary reference frame, which makes it more approaching from the base of the DTC. Thus, the stator flux and motor torque is controlled by sliding mode functions.

3.1 Switching surfaces selection

The knowledge of the controlled system model is absolutely necessary in sliding control design. In this paper, the chosen sliding manifolds are the electromagnetic torque and the square of stator flux. This latter plays an important role in the performance of a motor and is defined also to reduce the complexity [11,22]. The sliding surfaces is expressed as

$$S_1 = T_e^* - T_e, \tag{3}$$

$$S_2 = |\psi_s^*|^2 - |\psi_s|^2. \tag{4}$$

3.2 Control law definition

To generate the control law, the IM model (1) in Section 2 is used. The derivative of sliding surfaces can be written as

$$\dot{S} = F + DU, \tag{5}$$

$$\dot{S} = \begin{bmatrix} F_1 \\ F_2 \end{bmatrix} + \begin{bmatrix} D_1 \\ D_2 \end{bmatrix} \begin{bmatrix} U_{s\alpha} \\ U_{s\beta} \end{bmatrix}. \tag{6}$$

The derivative of the function of sliding surfaces S will be decoupled with respect to the reference stator voltage vectors (control outputs). By simple calculations, based on the mathematical model of the induction motor, Eq. (7) can be obtained.

$$\begin{cases} F_1 = -p\Big[c(\psi_{s\alpha} i_{s\beta} - \psi_{s\beta} i_{s\alpha}) + \omega_r(\psi_{s\alpha} i_{s\alpha} - \psi_{s\beta} i_{s\beta}) \\ \qquad -\dfrac{\omega_r}{\sigma L_s}|\psi_s|^2\Big], \\ F_2 = 2R_s(\psi_{s\alpha} i_{s\alpha} - \psi_{s\beta} i_{s\beta}), \end{cases} \tag{7}$$

where

$$c = -\left(\frac{R_s}{\sigma L_s} + \frac{R_r}{\sigma L_r}\right),$$

$$D = \begin{bmatrix} -p\left(i_{s\beta} - \dfrac{\psi_{s\beta}}{\sigma L_s}\right) & p\left(i_{s\alpha} - \dfrac{\psi_{s\alpha}}{\sigma L_s}\right) \\ -2\psi_{s\alpha} & 2\psi_{s\beta} \end{bmatrix}. \tag{8}$$

The switching function should be chosen in a manner to keep sliding mode behavior stable.

$$\dot{S} = -k_1 S - k_2 \mathrm{sign}(S). \tag{9}$$

When the switching surface $S = 0$ and by equalizing Eqs. (5) and (9), the general control law can be defined as

$$U = D^{-1}[-k_1 S - k_2 \mathrm{sign}(S)] + D^{-1} F. \tag{10}$$

The general control law in the sliding mode approach can be written as

$$U = \begin{bmatrix} U_{s\alpha} \\ U_{s\beta} \end{bmatrix} = \begin{bmatrix} U_{eq\alpha} \\ U_{eq\beta} \end{bmatrix} + \begin{bmatrix} U_{c\alpha} \\ U_{c\beta} \end{bmatrix}. \tag{11}$$

The two control parts can also be defined. The equivalent control can be expressed by

$$\begin{bmatrix} U_{eq\alpha} \\ U_{eq\beta} \end{bmatrix} = D^{-1} \begin{bmatrix} -F_1 \\ -F_2 \end{bmatrix}. \tag{12}$$

The discrete (commutation) control is defined as

$$\begin{bmatrix} U_{c\alpha} \\ U_{c\beta} \end{bmatrix} = D^{-1} \begin{bmatrix} -k_{11} S_1 - k_{12} \mathrm{sign}(S_1) \\ -k_{21} S_2 - k_{22} \mathrm{sign}(S_2) \end{bmatrix}, \tag{13}$$

where k_{11}, k_{12}, k_{21}, k_{22} are positive constants.

The global control law U will be expressed as

$$\begin{bmatrix} U_{s\alpha} \\ U_{s\beta} \end{bmatrix} = -D^{-1} \begin{bmatrix} F_1 + k_{11} S_1 + k_{12} \mathrm{sign}(S_1) \\ F2 + k_{21} S_2 + k_{22} \mathrm{sign}(S_2) \end{bmatrix}. \tag{14}$$

Then the reference voltages ($U_{s\alpha}$ and $U_{s\beta}$) have been generated in the stator reference frame.

The control law should be chosen so that it can attract the system trajectory to the sliding surface and satisfy the condition of Lyapunov stability [21]

$$V = \frac{1}{2} S^T S. \tag{15}$$

The derivative of Lyapunov function is given as

$$\dot{V} = S^T \dot{S}, \tag{16}$$

where $S^T = [\, S_1 \quad S_2 \,]$.

The stability condition $\dot{V} < 0$ has to be verified.

By substituting the switching function (Eq. 9) in the derivative of Lyapunov function, Eq. (17) can be obtained.

$$\dot{V} = S^T[-k_1 S - k_2 \mathrm{sign}(S)]. \tag{17}$$

Equation (17) can be written as

$$\dot{V} = -[k_1 S^T S + k_2 S^T \mathrm{sign}(S)]. \tag{18}$$

Equation (19) can be obtained.

$$\dot{V} = -[k_1 S^T S + k_2 |S|]. \tag{19}$$

For k_1 and $k_2 > 0$; $\dot{V} < 0$ ensures the stability of the sliding mode DTC.

3.3 Chattering phenomenon

The main drawback of the SMC is the chattering phenomenon caused by an infinite commutation, a disagreeable phenomenon which can excite high frequency harmonics and can also lead to damage of moving mechanical parts and heat losses in the electrical parts.

To solve this problem, the classical sign function is replaced by a smooth function defined as sigmoid function sigm (x) [12].

$$\text{sigm}(x) = \left(\frac{2}{1+\mathrm{e}^{\alpha x}}\right) - 1, \tag{20}$$

where α is a small positive constant which adjusts the sigmoid function slope.

4 Space vector modulation

To considerably reduce the torque and flux ripples, the generated reference voltages are modulated by the SVM unit to produce the command signal sin fixed switching frequency of the inverter. The principle of the SVM method is to predict the voltage vector and calculate it based on each of the three adjacent vectors in each sector. The application time for each vector can be obtained by vector calculations and the rest of the time period is spent by applying the null vector [6,20]. The space vector diagram for two-level inverter is shown in Fig. 1.

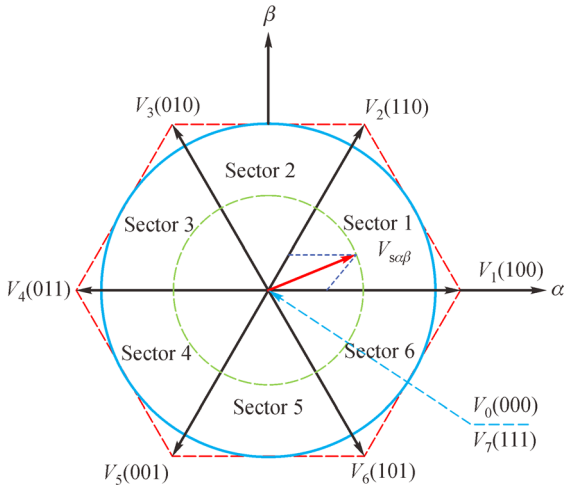

Fig. 1 Voltage space vector

The times T_1 and T_2 are determined by simple projections

$$T_1 = \frac{T_z}{2U_{dc}}\left(\sqrt{6}V_{s\beta ref} - \sqrt{2}V_{s\alpha ref}\right), \tag{21}$$

$$T_2 = \sqrt{2}\frac{T_z}{U_{dc}}V_{s\alpha ref}, \tag{22}$$

where T_1 and T_2 are the corresponding vector durations, T_z is the sampling period, and U_{dc} is the DC-bus voltage.

5 Speed regulation

The used speed controller is PI anti-windup for reference torque generation and to improve the performance of speed control by cancelling the integrator windup phenomenon which caused by saturation [23].

To overcome this phenomenon, the strategy is based on the difference between the control signal and the saturation limit to correct the integral action (Fig. 2). The difference value will be multiplied by gain (tracking time constant T_i) before becoming a feedback to the integrator.

6 SMO

6.1 SMO design

The goal of the SMO in this section is to construct stator flux components and use them for torque and speed estimation. The SMO bases on the state model of induction motor in rotor reference and stator flux ψ_s and current i_s as state variables [14].

$$\begin{cases} \dfrac{\mathrm{d}\psi_s}{\mathrm{d}t} = R_s i_s - j\omega_r + u_s \\ \dfrac{\mathrm{d}i_s}{\mathrm{d}t} = -\dfrac{1}{\sigma}\left(\dfrac{1}{T_r} + \dfrac{1}{T_s}\right)i_s + \dfrac{1}{\sigma L_s}\left(\dfrac{1}{T_r} - j\omega_r\right)\psi_s + \dfrac{1}{\sigma L_s}u_s. \end{cases} \tag{23}$$

where

$$T_s = \frac{L_s}{R_s}, T_r = \frac{L_r}{R_r}.$$

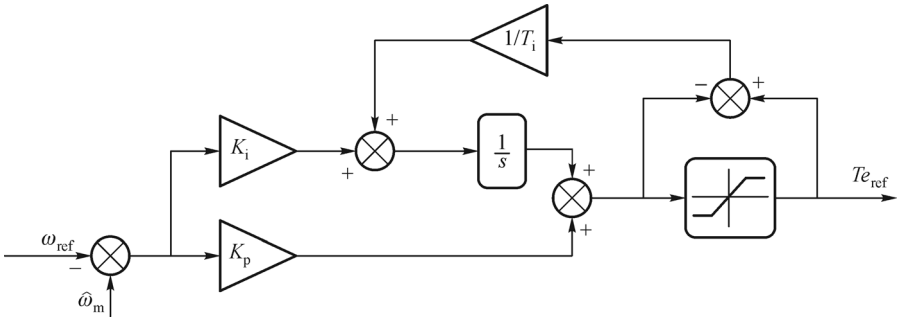

Fig. 2 Speed anti-windup PI controller

In this observer, the back-emf terms($\omega_r\psi_s$) is considered as disturbances. Then, the model of inherently observer (Fig. 3) can be expressed as

$$\begin{cases} \dfrac{\mathrm{d}\hat{\psi}_\mathrm{s}}{\mathrm{d}t} = R_\mathrm{s} i_\mathrm{s} + u_\mathrm{s} - K\mathrm{sign}(S_i) \\ \dfrac{\mathrm{d}\hat{i}_\mathrm{s}}{\mathrm{d}t} = -\dfrac{1}{\sigma}\left(\dfrac{1}{T_\mathrm{r}} + \dfrac{1}{T_\mathrm{s}}\right) i_\mathrm{s} + \dfrac{1}{\sigma L_\mathrm{s} T_\mathrm{r}} \psi_\mathrm{s} + \dfrac{1}{\sigma L_\mathrm{s}} u_\mathrm{s}, \\ \qquad -\dfrac{1}{\sigma L_\mathrm{s}} K\mathrm{sign}(S_\mathrm{i}) \end{cases} \quad (24)$$

where K is the observer switching gain, S_i is the sliding surface of the current error.

The PI controller is added just to impose more desired error convergence.

$$S_\mathrm{i} = \left(K_\mathrm{p} + \frac{K_\mathrm{i}}{s}\right)\left(\hat{i}_\mathrm{s} - i_\mathrm{s}\right). \quad (25)$$

6.2 Gain selection

The observer gain has to be large enough under stability condition from Lyapunov analysis. By using Lyapunov candidate function defined in Eq. (15) with IM and SMO models (Eq. 23), (Eq. 24) and during sliding mode $S_\mathrm{i} = 0$ and $\dot{S}_\mathrm{i} = 0$, K is given as

$$K > \max\left(\left|\frac{e_{\psi_{s\alpha}}}{T_\mathrm{r}} - \omega_\mathrm{r}\psi_{s\beta}\right|\left|\frac{e_{\psi_{s\beta}}}{T_\mathrm{r}} - \omega_\mathrm{r}\psi_{s\alpha}\right|\right), \quad (26)$$

where $e_{\psi_{s\alpha\beta}}$ is the flux error.

6.3 Speed estimator

The advantage of SMO is unrelated to rotor speed and when needed it can be estimated easily as

$$\hat{\omega}_\mathrm{r} = \hat{\omega}_\mathrm{s} - \hat{\omega}_\mathrm{sl} = \frac{1}{\psi_\mathrm{r}^2}\left(\frac{\mathrm{d}\hat{\psi}_{r\beta}}{\mathrm{d}t}\hat{\psi}_{r\alpha} - \frac{\mathrm{d}\hat{\psi}_{r\alpha}}{\mathrm{d}t}\hat{\psi}_{r\beta}\right) - \frac{R_\mathrm{s}\hat{T}_\mathrm{e}}{p\psi_\mathrm{r}^2}. \quad (27)$$

However, the computation of the rotor flux derivative is sensitive to noise. For this reason, the estimated speed has to be filtered by using LPF in order to be useable in this control algorithm.

6.4 Rotor flux estimator

In the stator flux observer or estimator, the rotor flux can be estimated from the stator flux and the measured current, as

$$\hat{\psi}_\mathrm{r} = \frac{L_\mathrm{r}\hat{\psi}_\mathrm{s} - L_\mathrm{s}L_\mathrm{r}\sigma i_\mathrm{s}}{M_\mathrm{sr}}. \quad (28)$$

The estimated torque can be calculated from Eq. (2).

The global control scheme of the proposed algorithm SM-DTC with SMO is shown in Fig. 4.

7 Simulation results

Based on the described theory in previous sections, the control scheme has been simulated by using the Matlab/Simulink software. The characteristics of the simulated three-phase 1.1 kW squirrel-cage induction motor are given in the Appendix. The simulation results are presented in two phases. The first phase is a comparative study of the proposed SM-DTC and the stator field oriented (SFOC) SVM-DTC using PI controllers. The second phase is the performance analysis of the control scheme with the SMO.

7.1 Comparative study of PI based SFOC SVM-DTC and SM-DTC

The comparative study of the proposed sliding mode DTC algorithm (SM-DTC) with SMO and the PI based stator flux oriented SVM-DTC is depicted in Figs. 5 to 10, where (a) for (SFOC) SVM-DTC and (b) for the SM-DTC. The stator phase current i_{sa} and electromagnetic torque are presented in Figs. 5 and 6. The estimated rotor speed with sense reversing at $t = 1$ s (1000 r/min; –1000 r/min) is illustrated in Fig. 6. The estimated stator flux is presented

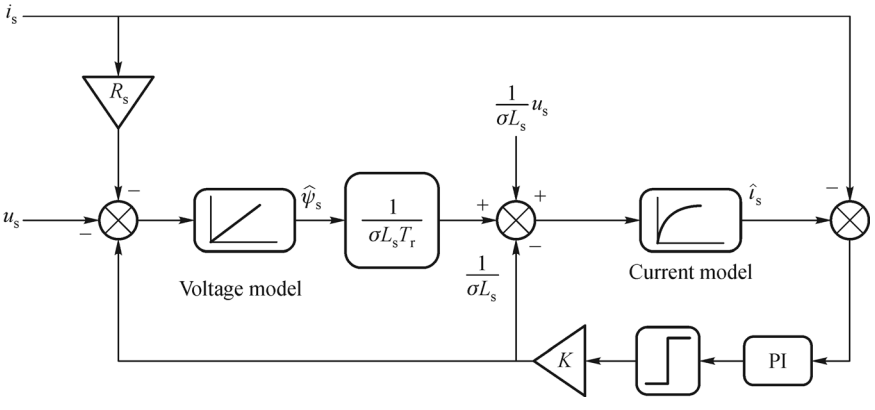

Fig. 3 Proposed sliding mode stator flux observer

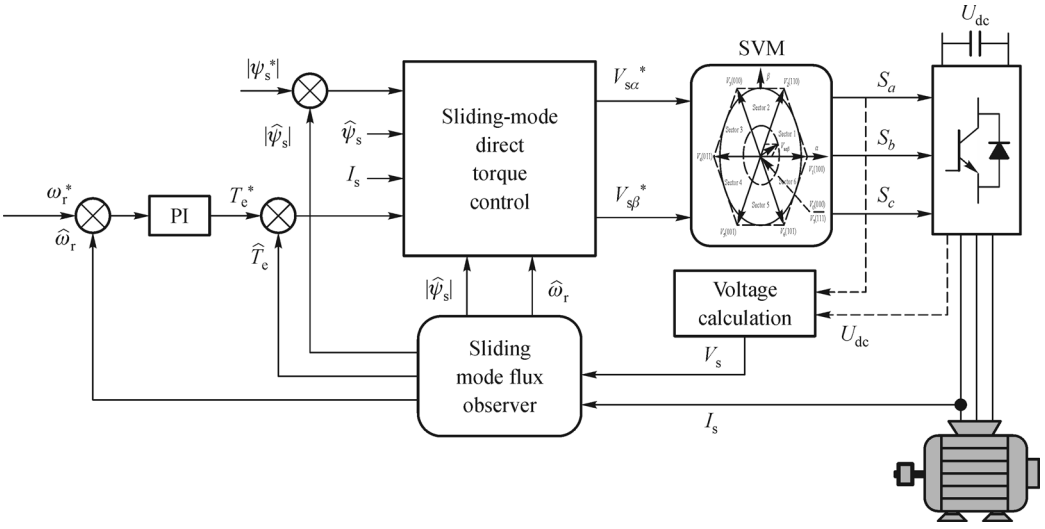

Fig. 4 Global diagram of sliding mode DTC (SM-DTC) with SMO

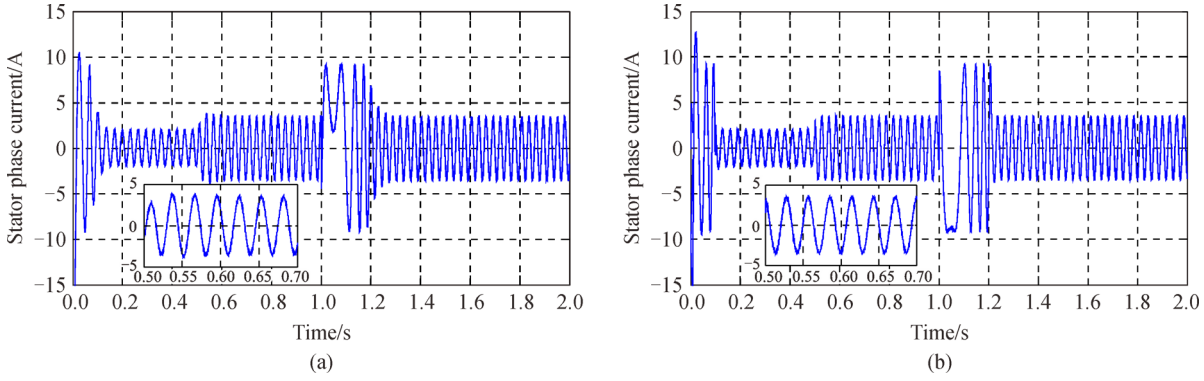

Fig. 5 Stator phase current
(a) For (SFOC) SVM-DTC; (b) for the SM-DTC

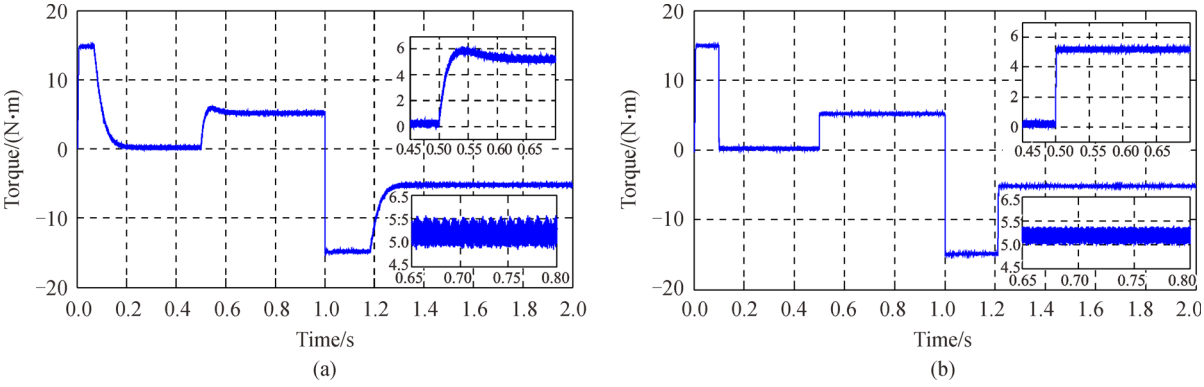

Fig. 6 Electromagnetic torque with load application of 5 N·m
(a) For (SFOC) SVM-DTC; (b) for the SM-DTC

in Figs. 8 to 10, where the flux magnitude is shown in Fig. 8, while the flux axes components and trajectory are shown respectively in Figs. 9 and 10. The rotor speed and flux magnitude under robustness test of stator resistance variation (R_s+ 100%) in low speed region (200 r/min) is demonstrated in Figs. 11 to 12.

Figure 5 illustrates the stator phase current $i_{s\alpha}$ with a load of 5 N·m introduced at 0.5 s for both PI based SVM-DTC

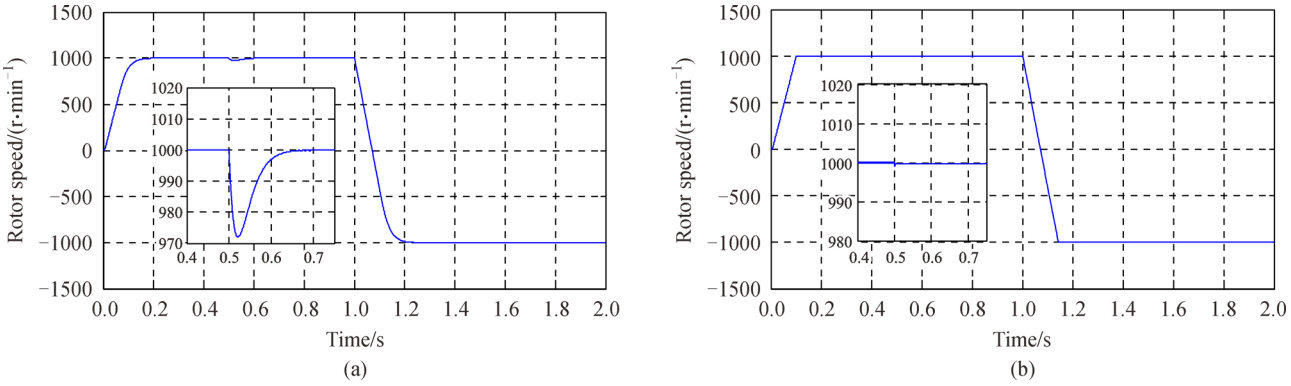

Fig. 7 Rotor speed response while sense reversing (1000 r/min; –1000 r/min)
(a) For (SFOC) SVM-DTC; (b) for the SM-DTC

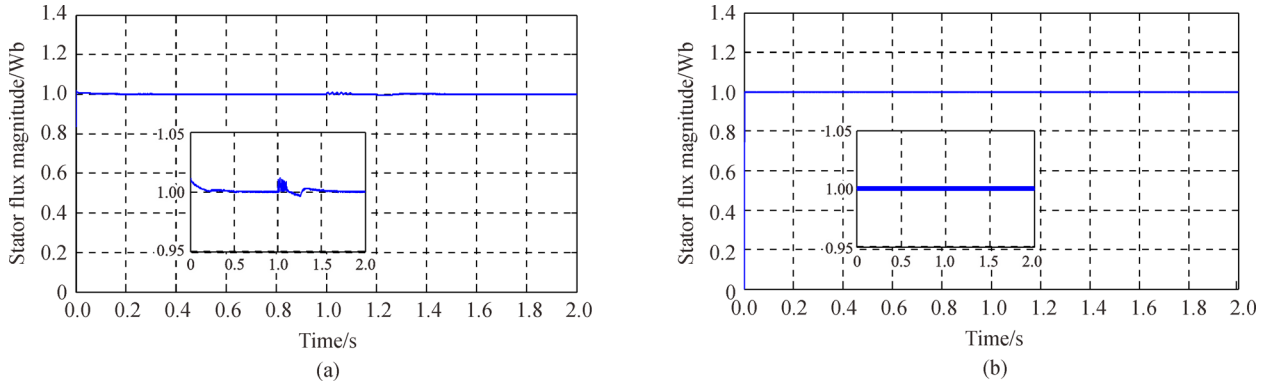

Fig. 8 Stator flux magnitude
(a) For (SFOC) SVM-DTC; (b) for the SM-DTC

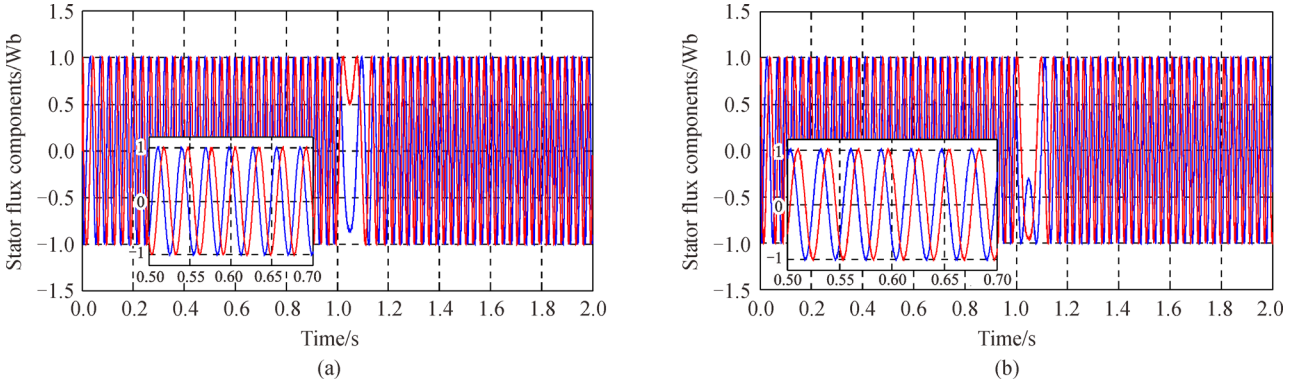

Fig. 9 Stator flux axis components (Wb)

and SM-DTC. The current shows good sinusoid waveform and reduced harmonics due to application of SVM. The SM-DTC presents a better current form with low chattering especially after the use of the sigmoid function. In Fig. 6, the comparison of electromagnetic torque responses is shown, where both torque responses show low ripple levels. It can also be seen that SM-DTC has a better dynamic and faster torque response during the startup and sense reversing states, in addition to the reducer chattering level. The rotor speed is exhibited in Fig.7 with an external load introduction of 5 N·m at $t = 0.5$ s and sense reversing (1000 r/min; –1000 r/min) at $t = 1$ s. From Fig.7(b), it can be noticed that the SM-DTC is more robust and has not affected greatly by the load application contrary to PI-SVM-DTC. Furthermore, it can also be observed that there exists a faster dynamic and better reference tracking during

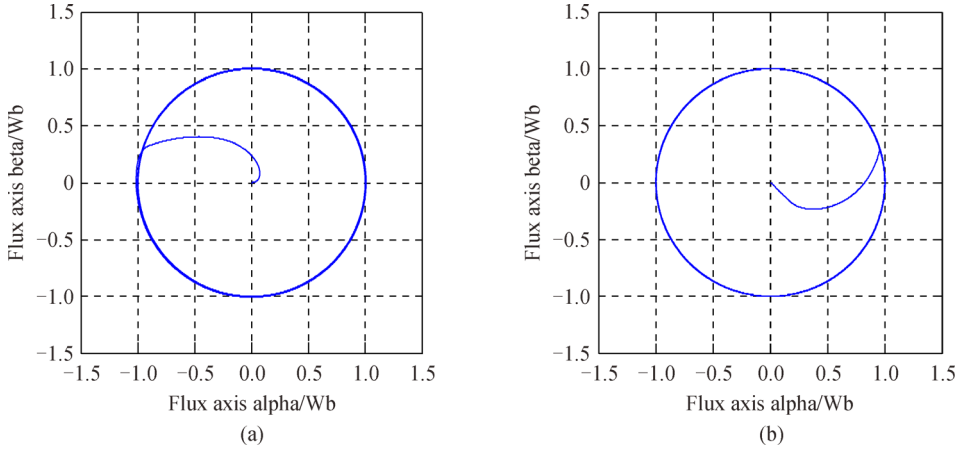

Fig. 10 Stator flux circle trajectory
(a) For (SFOC) SVM-DTC; (b) for the SM-DTC

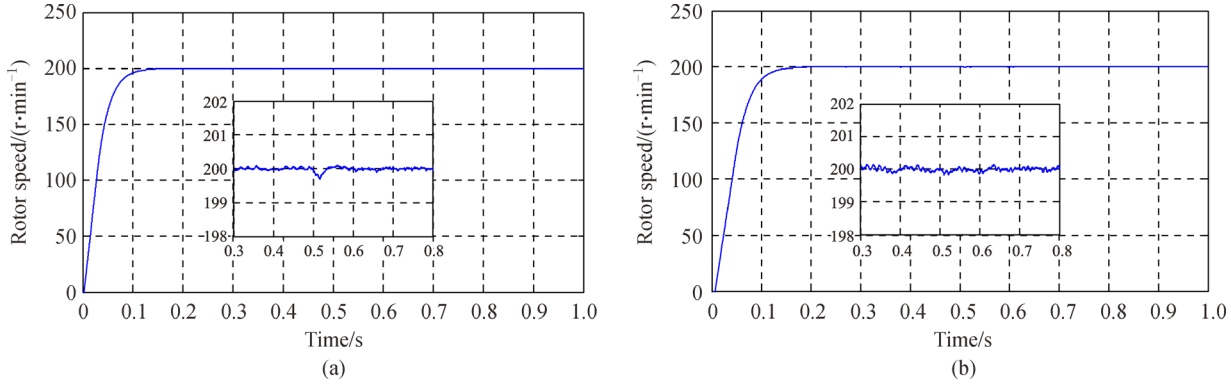

Fig. 11 Speed response at low region (200 r/min) with variation of stator resistance $R_s + 100\%$
(a) For (SFOC) SVM-DTC; (b) for the SM-DTC

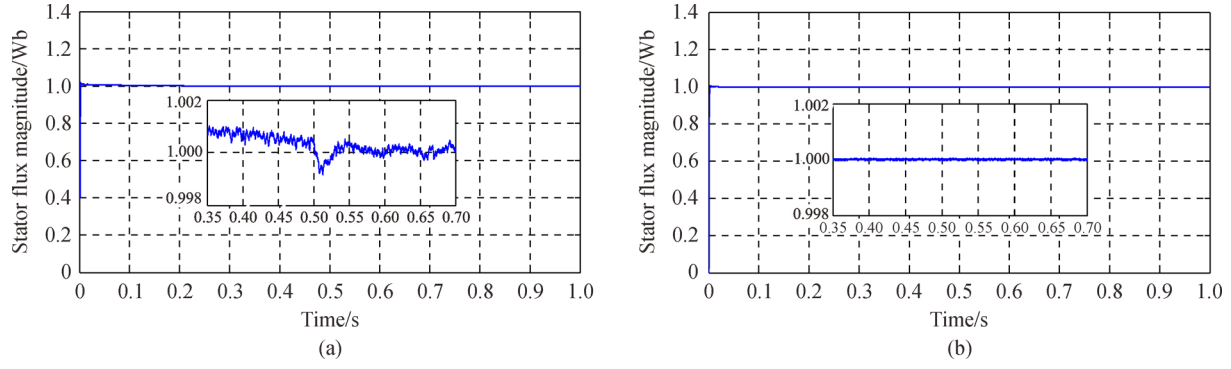

Fig. 12 Stator flux magnitude with variation of stator resistance $R_s + 100\%$
(a) For (SFOC) SVM-DTC; (b) for the SM-DTC

the speed reversing. The stator flux is presented in Figs. 8 to 10, which show respectively the flux magnitude, axes components and the circular flux trajectory. The two control techniques have a reduced ripple level stator flux, and the PI-SVM-DTC flux magnitude presents an overshot which has been influenced by the load and the reversing of speed direction. On the contrary, the SM-DTC flux magnitude has an accurate reference following (1 Wb) without any influence by the load variation. This indicates that a good decoupled control between flux and electro-

magnetic torque is achieved by the SM-DTC. Besides, the flux components and trajectory prove that the SM-DTC has a faster flux response. A robustness test is conducted which consists of parameter variation of the stator resistance R_s during low speed region of (200 r/min). Figures 11 and 12 illustrate the rotor speed and flux magnitude with increasing of (R_s + 100%) at $t = 0.5$ s. Unlike the PI based SVM-DTC, the proposed sliding mode DTC strategy does not have an apparent effect.

7.2 SMO performance analysis

Figures 13 to 16 show the estimated flux and speed with their estimation errors at various speed regions. A parameter variation test at low speed operation is conducted. Figure 13 show the flux magnitude with its estimation error. The speed response with different reference values and sense reversing is presented in Figs.14 and 15 (a). The speed estimation error is shown in Fig.15 (b) while the result of resistance variation test is given in Fig.16.

The observed flux obtained by the SMO has been illustrated in Figs. 8 to 10. The estimated flux magnitude at different speed regions with estimation error is presented in Fig. 13. The flux magnitude follows the reference and has a low ripple level, while the estimation error converges to zero in different speed operation between or less than ±0.01 Wb. This indicates the good observation accuracy. Figures 14 and 15 present the real and the estimated speed with speed reference. They show good reference tracking and superposition in all speed regions and sense reversing. The estimation error of rotor speed is shown Fig. 15(b), which always converges to zero in all speed regions. This indicates the robustness of the speed estimator during different operation modes. Figure 16 shows the observed flux magnitude and rotor speed with variation of R_s and R_r + 100% at 0.5 s. It is seen that the sensitivity of flux and speed from R_r variation is not apparent. In R_s variation, the influence and the error are not so considerable and have been recovered quickly because of the robustness of the SMO which can be improved in the future work using the adaptive strategy.

8 Experimental results

The proposed control scheme implemented in Matlab/Simulink is verified by the experimental tests. The real time control is done in the laboratory equipped by the dSpace 1104 board. The implementation ground of

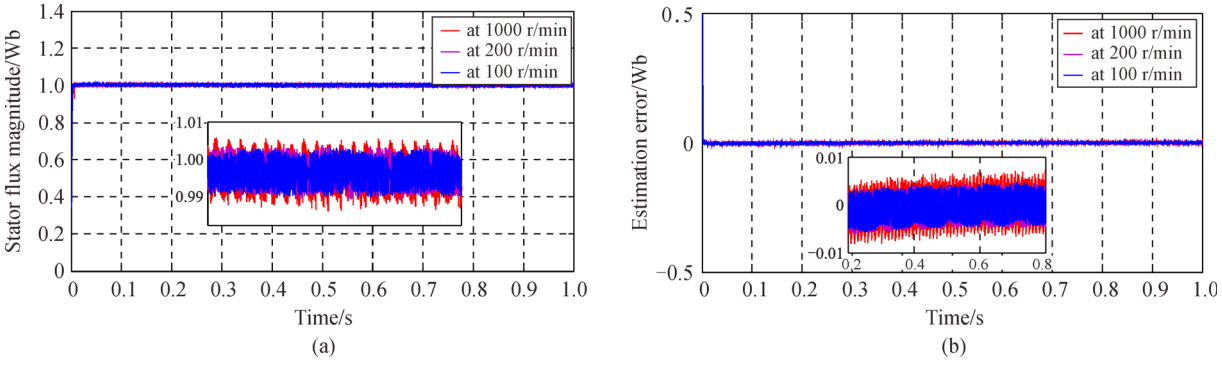

Fig. 13 Estimated flux magnitude at different speed regions with estimation error
(a) Stator flux magnitude; (b) estimation error

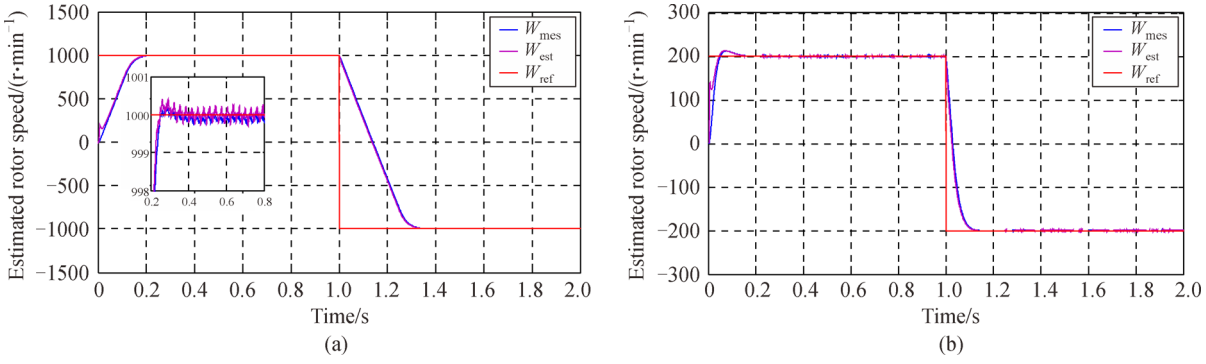

Fig. 14 Estimated speed at different references and sense reversing (r/min)
(a) For high speed region (1000 r/min); (b) for low speed region (200 r/min)

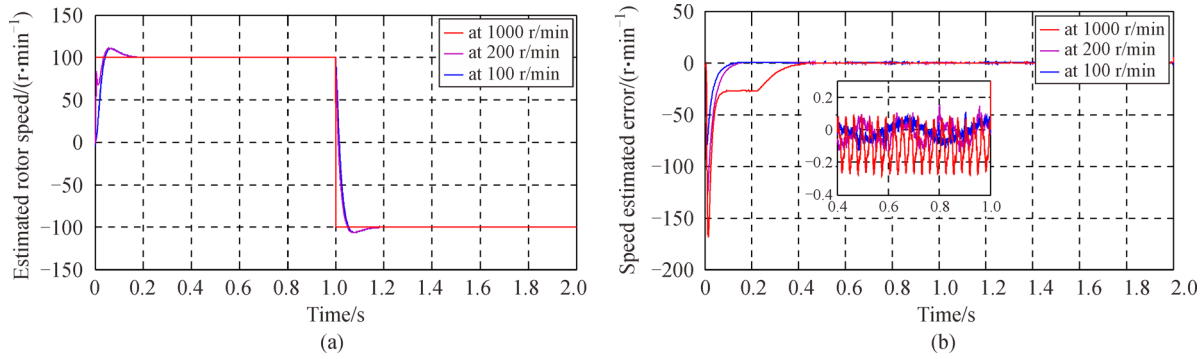

Fig. 15 Estimated speed at low speed region (100 r/min; −100 r/min) and estimation error
(a) for low speed region (100 r/min); (b) estimation error

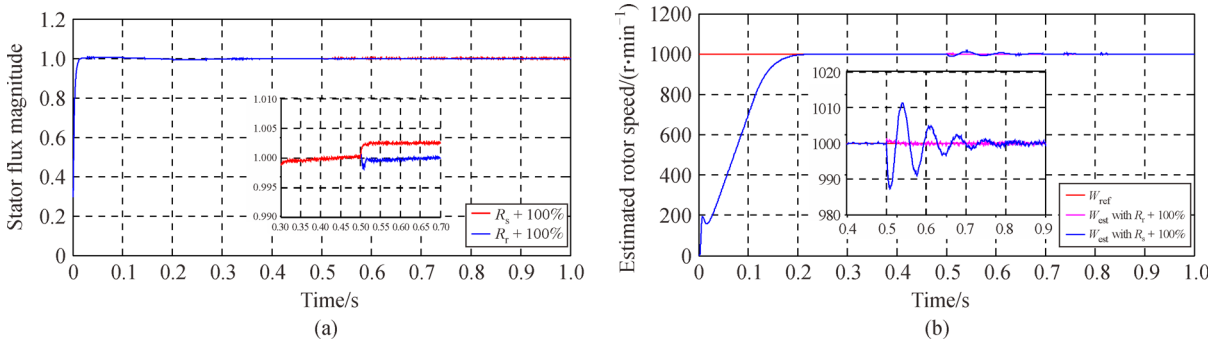

Fig. 16 Flux magnitude with parameter variations test R_s and R_r of + 100%
(a) Stator flux magnitude; (b) rotor speed

induction motor drive is essentially composed, as shown in Fig. 17, of a squirrel-cage IM 1.1 kW; a power electronics Semikron converter composed of a rectifier and an IGBT inverter; a speed sensor incremental encoder used in order to check and compare the real speed with the estimated speed from sensorless algorithm; dSpace dS 1104 board; control desk software plugged in personnel computer; a magnetic powder brake with a load control unit; Hall type current sensors. (To reduce the cost of the control system, the phase voltages is estimated from DC-bus voltage and inverter switching states (S_a, S_b, S_c) instead of using voltage sensors [5,20]); voltage sensors; and a numerical

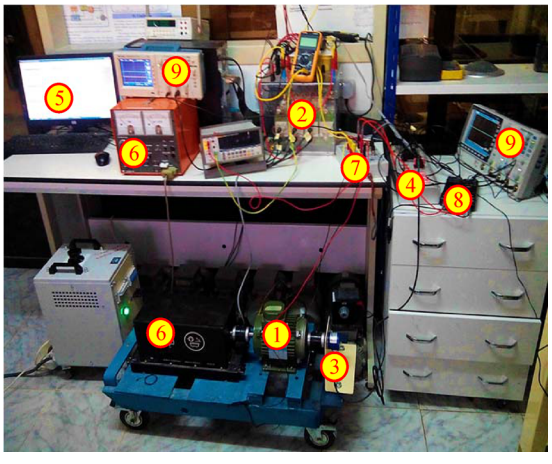

Fig. 17 Experimental setup

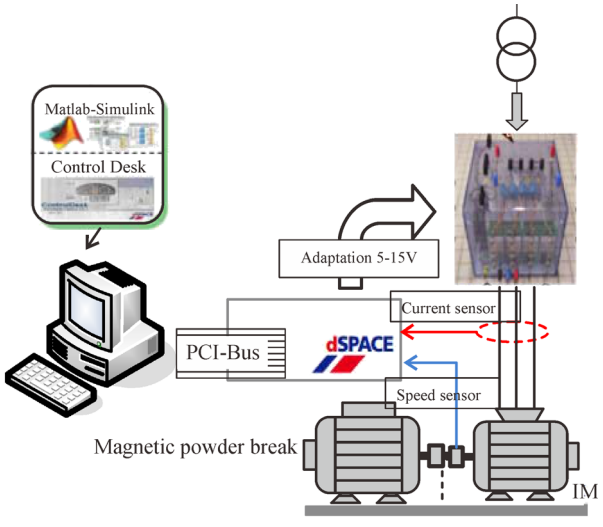

Fig. 18 Simplified real time setup scheme

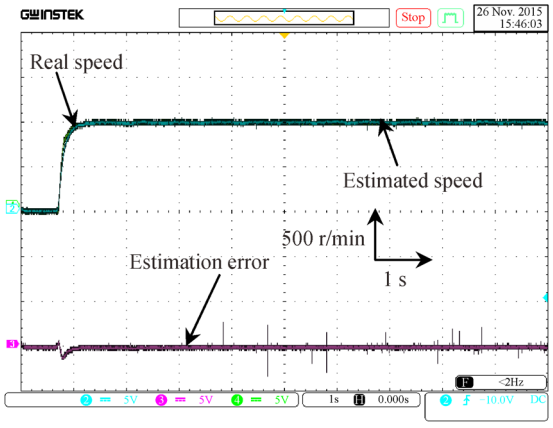

Fig. 19 Startup state: real and estimated speed, with estimation error (r/min)

oscilloscope. Figure 18 presents a simplified setup scheme.

Figure 19 shows the rotor speed (1div = 500 r/min) in the startup state (0 to 1000 r/min). From Fig. 19, a good and fast response similar to the simulation test can be noticed. Figure 20 illustrates the speed estimation in sense reversing with variable reference (trapezoidal). The reference tracking and the estimation accuracy are good. Both Fig. 19 and Fig. 20 show a superposition between the real and the estimated speed in the two cases, in the startup and sense reversing. The estimation error converges to zero, which indicates the accuracy and the robustness of the speed estimator.

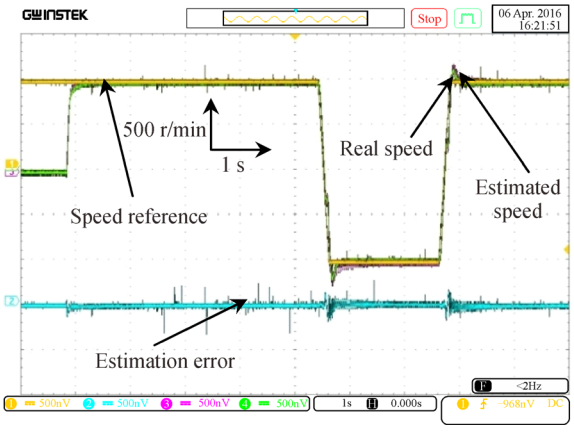

Fig. 20 Speed variation: real and estimated speed with estimation error (r/min)

Figures 21 to 24 show the steady state of the induction motor without load. Figure 21 shows the rotor speed and stator phase current with reduced ripple level and good sinusoid waveform. The observed stator flux obtained from the SMO is shown in Figs. 22 to 24, with the stator flux magnitude, components and circle trajectory displayed, respectively. The flux magnitude with the estimation error

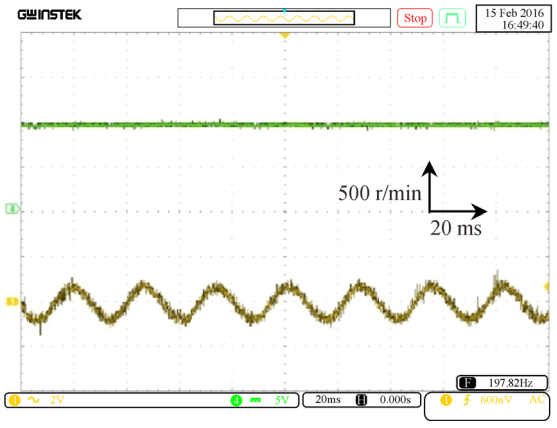

Fig. 21 Steady state: rotor speed, stator phase current (A)

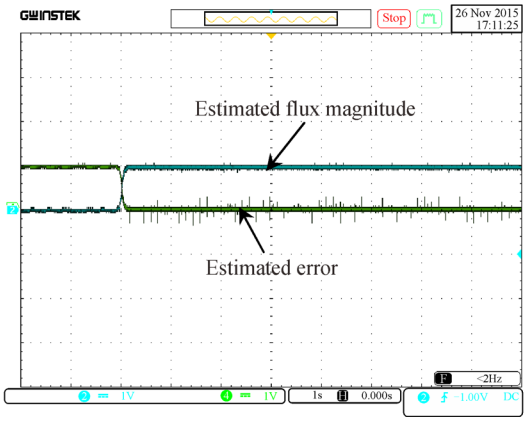

Fig. 22 Stator flux magnitude with estimation error(Wb)

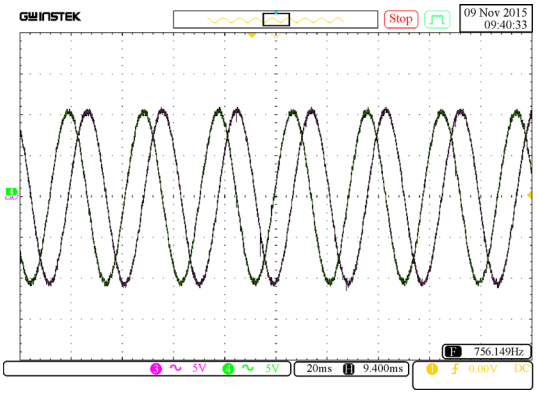

Fig. 23 Stator flux axes components

are shown in Fig. 22, where the error converges to zero when the flux magnitude follows its reference 1 Wb (1div = 1 Wb) with a low ripple level.

Figure 23 shows the flux axes components (1div = 0.5 Wb), with a good sinusoid waveform and low ripples. The trajectory is presented in Fig. 24.

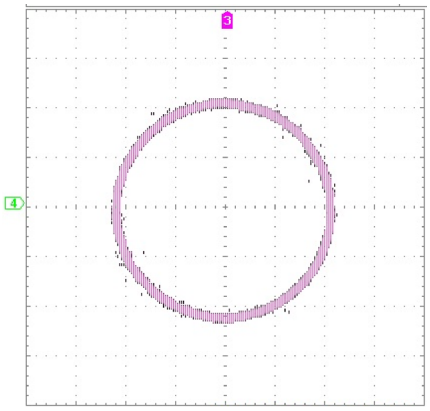

Fig. 24 Stator flux circle trajectory

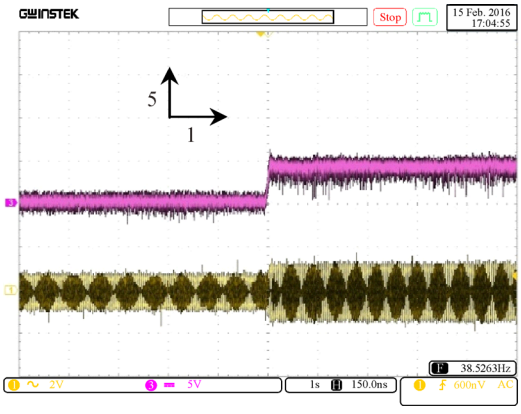

Fig. 25 Load introduction: torque (N·m), stator current (A)

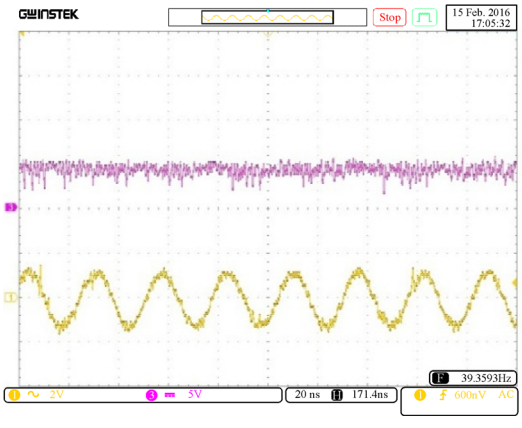

Fig. 26 Load introduction: torque, stator current (A) (ZOOM)

Figures 25 and 26 illustrate the load application of 5 N·m (1div = 5 N·m) with stator phase current. These two figures show the response of the motor to the load introduction with reduced ripple levels of electromagnetic torque due the use of the space vector modulation. Figures 27 and 28 show the performance analysis of the observer in

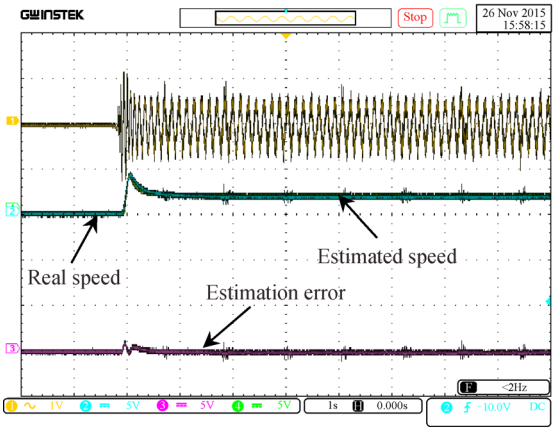

Fig. 27 Low speed operation (200 r/min): stator phase current, estimated and real speed, estimation error

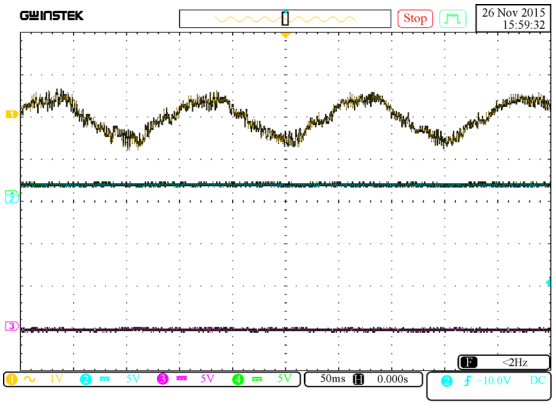

Fig. 28 Low speed operation (200 r/min): stator phase current, estimated and real speed, estimation error (ZOOM)

the low speed region of (200 r/min). These two figures illustrate, from the top to the bottom, the stator phase current, the real and estimated rotor speed, and the estimation error. The current presents an acceptable waveform and ripple levels in the low speed region. The speed estimation is also accurate and good superposition with the real speed, while the error converges to zero in the steady state. The proposed control method is an improved DTC and estimation strategy based totally on the sliding mode approach. More than known robustness of the sliding mode, it presents the advantages of both classical and SVM-DTC such as fast response, simple strategy using a stationary frame, in addition to the reduced flux and torque ripples. Besides, the associated SMO shows a good estimation accuracy in different tests.

9 Conclusions

The presented work describes an enhanced control and

observation algorithm based on the sliding mode strategy, which is composed of sliding mode DTC SM-DTC with space vector modulation and SMO for stator flux, torque and speed estimation.

In order to overcome the drawbacks of DTC and SVM-DTC and obtain a high performance control, the SMC has been designed based on the torque and flux errors. The coupling of DTC principles with SMC has achieved an optimized control strategy with good tracking accuracy and strong robustness to different disturbances and parameters variation. Because of applying constant switching frequency archived by the space vector modulation, the torque, flux and current ripple levels are reduced.

The sliding mode DTC scheme has many advantages which are verified by simulation and experimental tests such as high robustness against parameter variation and load disturbance. This control scheme still preserves the fast dynamic response of the DTC with good performance at different speed regions. Moreover, it has a more reduced structure complexity than the SVM-DTC.

The association of the control scheme with an observer also increases the reliability and decreases the cost of using sensors and installation. Since the presented SMO does not need the speed adaptation mechanism, it does not have an influence on observation contrary to other structures. The performances and effectiveness of SMO have also been verified. The results show good accuracy and acceptable errors level in both speed and flux estimation, robustness in different tests such as load application, speed variation, and low speed operation. Therefore, the improved sliding mode DTC is a good solution in general to overcoming the drawbacks of DTC and getting robust control. The combination of this control with a robust sensorless algorithm can give higher performances for induction motor electrical drive.

Notations

The parameters of the used induction motor in simulation and experimental implementation in SI units are 1.1 kW, 50 Hz, $p = 2$, $R_s = 6.75\ \Omega$, $R_r = 6.21\ \Omega$, $L_s = L_r = 0.5192$ H, $M_{sr} = 0.4957$ H, $f_r = 0.002$ SI, $J = 0.01240\ \mathrm{kg \cdot m^2}$.

References

1. Casadei D, Profumo F, Tani A. FOC and DTC: two viable schemes for induction motors torque control. IEEE Transactions on Power Electronics, 2002, 17(5): 779–787
2. Ren Y, Zhu Z. Enhancement of steady-state performance in direct torque controlled dual-three phase permanent magnet synchronous machine drives with modified switching table. IEEE Transactions on Industrial Electronics, 2015, 62(6): 3338–3350
3. Douiri M, Cherkaoui M. Comparative study of various artificial intelligence approaches applied to direct torque control of induction motor drives. Frontiers in Energy, 2013, 7(4): 456–467
4. Alsofyani I, Idris N. Simple flux regulation for improving state estimation at very low and zero speed of a speed sensorless direct torque control of an induction motor. IEEE Transactions on Power Electronics, 2016, 31(4): 3027–3035
5. Hafeez M, Uddin M, Rahim N A. Ping H W. Self-tuned NFC and adaptive torque hysteresis-based DTC scheme for IM drive. IEEE Transactions on Industry Applications, 2014, 50(2): 1410–1420
6. Lascu C, Boldea I, Blaabjerg F. A modified direct torque control for induction motor sensorless drive. IEEE Transactions on Industry Applications, 2000, 36(1): 122–130
7. Habetler T, Profumo F, Pastorelli M, Tolbert L. Direct torque control of induction machines using space vector modulation. IEEE Transactions on Industry Applications, 1992, 28(5): 1045–1053
8. Kumsuwan Y, Premrudeepreechacharn S, Toliyat H. Modified direct torque control method for induction motor drives based on amplitude and angle control of stator flux. Electric Power Systems Research, 2008, 78(10): 1712–1718
9. Zaafouri A, Regaya C, Azza H, Châari A. DSP-based adaptive back stepping using the tracking errors for high-performance sensorless speed control of induction motor drive. ISA Transactions, 2016, 60: 333–347
10. Choi Y, Choi H, Jung J. Feedback linearization direct torque control with reduced torque and flux ripples for IPMSM drives. IEEE Transactions on Power Electronics, 2016, 31(5): 3728–3737
11. Orlowska-Kowalska T, Tarchala G, Dybkowski M. Sliding-mode direct torque control and sliding-mode observer with a magnetizing reactance estimator for the field-weakening of the induction motor drive. Mathematics and Computers in Simulation, 2014, 98: 31–45
12. Lee H, Lee J. Design of iterative sliding mode observer for sensorless PMSM control. IEEE Transactions on Control Systems Technology, 2013, 21(4): 1394–1399
13. Utkin V. Sliding mode control design principles and applications to electric drives. IEEE Transactions on Industrial Electronics, 1993, 40(1): 23–36
14. Lascu C, Boldea I, Blaabjerg F. A class of speed-sensorless sliding-mode observers for high-performance induction motor drives. IEEE Transactions on Industrial Electronics, 2009, 56(9): 3394–3403
15. Yazdanpanah R, Soltani J, Arab Markadeh G. Nonlinear torque and stator flux controller for induction motor drive based on adaptive input-output feedback linearization and sliding mode control. Energy Conversion and Management, 2008, 49(4): 541–550
16. Saghafinia A, Ping H, Uddin M, Gaeid K. Adaptive fuzzy sliding-mode control into chattering-free IM drive. IEEE Transactions on Industry Applications, 2015, 51(1): 692–701
17. Lascu C, Boldea I, Blaabjerg F. Direct torque control of sensorless induction motor drives: a sliding-mode approach. IEEE Transactions on Industry Applications, 2004, 40(2): 582–590
18. Barambones O, Alkorta P. Position control of the induction motor using an adaptive sliding-mode controller and observers. IEEE Transactions on Industrial Electronics, 2014, 61(12): 6556–6565
19. Fan Y, Zhang L, Cheng M, Chau K. Sensorless SVPWM-FADTC of a new flux-modulated permanent-magnet wheel motor based on a wide-speed sliding mode observer. IEEE Transactions on Industrial Electronics, 2015, 62(5): 3143–3151
20. Ammar A, Bourek A, Benakcha A. Modified load angle direct torque control for sensorless induction motor using sliding mode

flux observer. In: 4th International Conference on Electrical Engineering (ICEE). Boumerdes, Algeria, 2015

21. Hassan A, El-Sawy A, Mohamed Y, Shehata E. Sensorless sliding mode torque control of an IPMSM drive based on active flux concept. Alexandria Engineering Journal, 2012, 51(1): 1–9
22. Henini N, Nezli L, Tlemçani A, Mahmoudi M O. Improved multi-machine multiphase electric vehicle drive system based on new SVPWM strategy and sliding mode-direct torque control. Nonlinear Dynamics and Systems Theory, 2011, 11(4): 425–438
23. Yang M, Tang S, Xu D. Comments on "Antiwindup strategy for PI-type speed controller". IEEE Transactions on Industrial Electronics, 2015, 62(2): 1329–1332